Doppler-Free vs. Doppler-Broadened Two-Photon Absorption in Cesium: Experimental Fluorescence Comparison for the $6S_{1/2} \rightarrow 8S_{1/2}$ Transition

Catalina Fuentes Rubio,* Jose Ricardo Mejía Mora, and Mayerlin Núñez Portela†

Grupo de Óptica Cuántica, Departamento de Física,

Universidad de los Andes, Bogotá, Colombia

(Dated: May 23, 2026)

Two-photon absorption (TPA) in atomic vapors is a key process in frequency metrology, nonlinear spectroscopy, and the study of quantum light–matter interactions such as entangled two-photon absorption (ETPA). At low photon fluxes, however, detecting the weak fluorescence signal associated with TPA remains experimentally challenging. In this work we study the $6S_{1/2} \rightarrow 8S_{1/2}$ two-photon transition in a cesium vapor cell at 822 nm using both Doppler-broadened (DB) and Doppler-free (DF) excitation schemes. For the DB configuration, a single co-propagating linearly polarized beam is used. For the DF configuration, two counter-propagating beams of identical frequency are produced by retroreflection, and both linear and circular polarization schemes are implemented. The fluorescence spectra are fitted with Gaussian (DB) and Lorentzian (DF) profiles to extract the peak amplitude and the full-width at half-maximum (FWHM). We find an amplitude ratio $F_{\mathrm{DF}} : F_{\mathrm{DB}} \approx 3 : 1$ between the two schemes, a DB linewidth of (808 ± 3) MHz consistent with a cell temperature of (318.3 ± 0.8) K, and DF linewidths of 5.96 ± 0.01 MHz (linear polarization) and 10.14 ± 0.01 MHz (circular polarization), to be compared with the natural linewidth of 1.53 MHz for the $8S_{1/2}$ state. A temperature-dependent study of the DF signal between 25°C and 50°C shows the expected growth of the fluorescence peak with cesium vapor density. These results establish a baseline for future TPA and ETPA experiments in cesium, where precise fluorescence detection at low photon fluxes is essential.

* c.fuentesr@uniandes.edu.co

† m.nunez@uniandes.edu.co

I. INTRODUCTION

Two-photon absorption (TPA) is a nonlinear optical process in which an atom or molecule simultaneously absorbs two photons to reach an excited state whose energy equals the sum of the two photon energies. Unlike one-photon absorption (OPA), where a single photon carries the full transition energy, TPA proceeds through a *virtual intermediate state* that does not correspond to any real eigenstate of the system [2]. First analyzed theoretically by Göppert-Mayer in 1931 [1], TPA has since become a fundamental tool in nonlinear and quantum optics, with applications ranging from multiphoton microscopy [3] to atomic clocks and frequency metrology [4].

The TPA transition probability depends quadratically on the laser intensity, $R_{\mathrm{TPA}} \propto I^2$, in contrast to the linear dependence of OPA [2]. Resonance is reached when the total energy of the two incoming photons matches the energy difference between the initial and final atomic states,

$$E_f - E_i \;=\; h\nu_1 + h\nu_2, \tag{1}$$

which for two identical (degenerate) photons of frequency ν_L reduces to $\omega_{fi} = 2\omega_L$.

In this work the active medium is atomic cesium. The simple alkali electronic structure of Cs allows a hydrogen-like theoretical treatment of its transitions and makes it a standard test bed for high-resolution atomic spectroscopy [5]. We focus on the $6S_{1/2} \rightarrow 8S_{1/2}$ two-photon transition, accessible with infrared diode lasers near 822 nm. The relevant level structure and decay channels are summarized in Fig. 1. Once the atom is excited to the $8S_{1/2}$ state, it can decay through the intermediate $7P_{3/2}$, $7P_{1/2}$, $6P_{3/2}$ and $6P_{1/2}$ levels back to the $6S_{1/2}$ ground state, emitting fluorescence photons whose detection provides a direct measure of the TPA process [5].

In a thermal gas, the resolution of any absorption experiment is limited by the Doppler effect: each atom moving with axial velocity v_z along the laser propagation direction perceives a frequency-shifted field. To first order in v_z/c, the perceived frequency is

$$\nu' \;=\; \nu_L\Big(1 - \frac{v_z}{c}\Big). \tag{2}$$

Because the atomic velocities follow a Maxwell–Boltzmann distribution, absorption occurs over a range of shifted frequencies, producing a Gaussian spectral profile of full-width at half-maximum (FWHM) [6]

$$\delta\nu_D \;=\; \frac{\nu_0}{c}\sqrt{\frac{8k_BT\ln 2}{M}}, \tag{3}$$

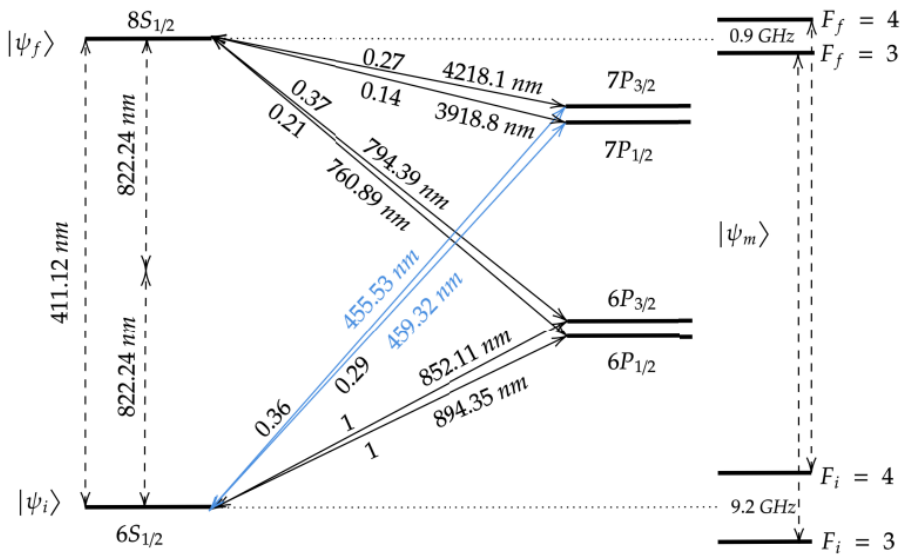

FIG. 1. Energy-level diagram of atomic cesium showing the levels relevant to this work. Solid arrows indicate one-photon transitions with their wavelengths and branching ratios, while the dashed lines indicate the two-photon excitation pathway $6S_{1/2} \rightarrow 8S_{1/2}$ at 822.24 nm. The hyperfine splittings of the ground and excited states are also indicated [5].

where k_B is Boltzmann's constant, T is the gas temperature, M is the atomic mass and ν_0 is the transition frequency. For the $6S_{1/2} \rightarrow 8S_{1/2}$ Cs transition near room temperature, $\delta\nu_D$ is of order ~ 1 GHz, much larger than the natural linewidth of the upper state (~ 1.5 MHz), so that the observed line is strongly Doppler-broadened (DB) and its peak amplitude is correspondingly reduced even though the integrated absorption is conserved [5].

One of the ways to suppress Doppler broadening in TPA experiments is the use of *counter-propagating beams* of identical frequency, originally proposed by Cagnac, Grynberg, and Biraben [7]. Consider an atom moving with axial velocity v_z illuminated by two counter-propagating beams of laboratory frequency ν_L. In the atomic rest frame the two beams are perceived as

$$\nu_1 = \nu_L\left(1 - \frac{v_z}{c}\right), \qquad \nu_2 = \nu_L\left(1 + \frac{v_z}{c}\right), \tag{4}$$

so that if the atom absorbs one photon from each beam the total absorbed energy is

$$E_f - E_i \;=\; h\nu_1 + h\nu_2 \;=\; 2h\nu_L, \tag{5}$$

with the velocity-dependent terms cancelling exactly. The principle is illustrated in Fig. 2. As a consequence, atoms of all velocity classes contribute to the absorption at the same resonance

frequency, and the resulting spectral line is no longer Doppler-broadened but limited (in the ideal case) only by the natural Lorentzian linewidth of the transition [4].

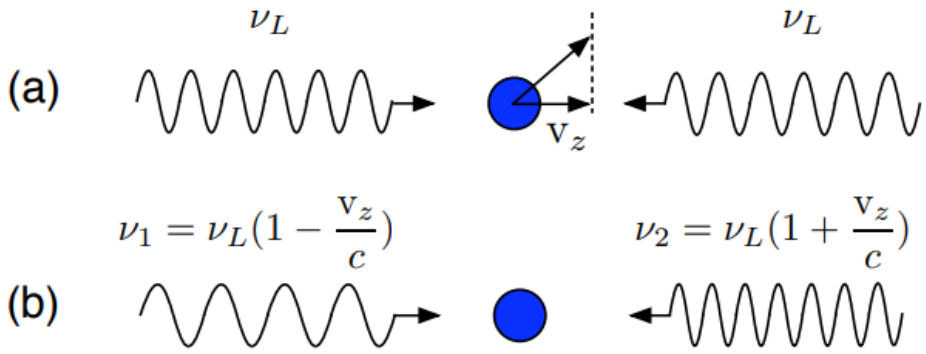

FIG. 2. Principle of Doppler-free two-photon absorption. (a) In the laboratory frame, two counter-propagating beams of the same frequency ν_L interact with an atom moving at velocity v_z. (b) In the atomic rest frame the two beams are perceived at $\nu_1 = \nu_L(1 - v_z/c)$ and $\nu_2 = \nu_L(1 + v_z/c)$. When one photon is absorbed from each beam, the opposite Doppler shifts cancel and the resonance condition becomes velocity-independent. Adapted from Ref. [8].

The cancellation of the Doppler shift in the DF configuration concentrates the entire absorption probability into a frequency window narrower than the inhomogeneous Doppler profile by roughly $\delta\nu_D/\Gamma_{\rm nat} \sim 10^2$–$10^3$. Because the total integrated absorption remains essentially the same, the DF fluorescence peak is correspondingly *taller* than its DB counterpart. This intensity gain is particularly relevant for low-photon-flux experiments such as entangled two-photon absorption (ETPA), where the small number of detected photons makes the signal-to-noise ratio the limiting factor for measurement [9].

The selection rules of the two-photon $6S_{1/2} \rightarrow 8S_{1/2}$ transition further constrain the choice of polarization. For the transition $\Delta L = 0$ the change in total angular momentum projection along the quantization axis must satisfy $m_1 + m_2 = 0$, where $m_{1,2}$ are the angular momenta carried by each absorbed photon [7]. For linearly polarized π light each photon carries $m = 0$ and the selection rule is trivially satisfied. For circularly polarized light a photon co-propagating with the quantization axis carries $m = +1$ (σ^+) or $m = -1$ (σ^-). Therefore, in a counter-propagating configuration with quarter-wave plates placed before and after the cell, an atom sees σ^+ from one direction and σ^- from the other, again satisfying $m_1 + m_2 = 0$, while two co-propagating photons of the same circular polarization would give $m_1 + m_2 = \pm 2$ and would not drive the transition.

The polarization geometry therefore acts as an additional discriminator between the DF and DB pathways.

Building on the theoretical and experimental characterization of the classical TPA cross section of this transition reported recently by Caracas Núñez *et al.* [5], the present work moves from the DB regime to the DF regime as a first step toward fluorescence detection at low photon fluxes. Concretely, we record and compare the two-photon induced fluorescence (TPIF) spectrum of the $6S_{1/2} \rightarrow 8S_{1/2}$, $F = 4 \rightarrow F = 4$ transition under three configurations of practical interest: (i) DB excitation with linear polarization, (ii) DF excitation with linear polarization, and (iii) DF excitation with circular polarization. We extract the peak amplitude and the FWHM of each spectrum, infer the vapor temperature from the DB Gaussian width, and study how the DF fluorescence peak depends on the cesium vapor temperature between 22°C and 50°C. The DF/DB intensity ratio obtained here quantifies the gain expected from a Doppler-free strategy in the eventual measurement of ETPA in atomic cesium [9].

II. EXPERIMENTAL METHODOLOGY

The experimental setup is based on a continuous-wave external-cavity diode laser tuned to the cesium $6S_{1/2} \rightarrow 8S_{1/2}$ two-photon resonance near 822.24 nm. The same basis is used in all three configurations: the only differences between the DB and DF schemes are the addition of a retroreflecting mirror and a refocusing lens after the cell, and the addition (in the circular-polarization case) of two quarter-wave plates, one before and one after the cesium cell.

A. Optical layout common to all configurations

A schematic of the common optical layout is shown in Fig. 3. The diode laser is mounted in a Littrow external-cavity geometry, with a reflective diffraction grating (RD, 1200 lines/mm) selecting the first diffraction order and feeding it back into the laser cavity to ensure single-longitudinal-mode operation [10]. The laser wavelength is monitored continuously with a high-precision wavelength meter (WLM) fed by a fiber coupler (CFC-2X-B); a beam sampler (BS) directs a small fraction of the output to this monitoring arm. After the main beam passes through an optical isolator (OI) that protects the laser from back-reflections and fixes a linear polarization, a divergent telescope formed by lenses f_1 (focal length -25 mm) and f_2 (-100 mm) magnifies the beam. A long-pass filter (LPF) blocks ambient visible light, and a converging lens f_3 ($+50$ mm) focuses the beam inside

the cesium vapor cell (GC25075-CS). The beam waist at the focus inside the cell was measured to be

$$w_{0,x} = (15.6 \pm 0.4)\ \mu\text{m}, \qquad w_{0,y} = (12.7 \pm 0.4)\ \mu\text{m}.$$

The fluorescence emitted from the excitation region is collected perpendicularly to the propagation axis by a photomultiplier tube (PMT) through a spectral filter (SF) that selects only the relevant decay channels (cf. Fig. 1) and rejects scattered 822 nm light. The PMT photocurrent is read by a counting electronics chain synchronized with the laser frequency scan controlled from a computer.

The temperature of the cesium cell is regulated by a resistive heater and a PID controller, allowing measurements between room temperature and $\sim 60°\text{C}$. The cesium number density at each temperature is set by the saturated vapor pressure curve [11].

B. Doppler-broadened TPA – linear polarization

For the DB configuration only the elements shown in Fig. 3 are used. A single linearly polarized beam (π polarization with $m = 0$) is focused into the cesium cell and the fluorescence is recorded as a function of the laser frequency. Because only one beam interacts with the atoms, the two absorbed photons are co-propagating, both Doppler shifts have the same sign, and the fluorescence spectrum displays the full Gaussian Doppler profile.

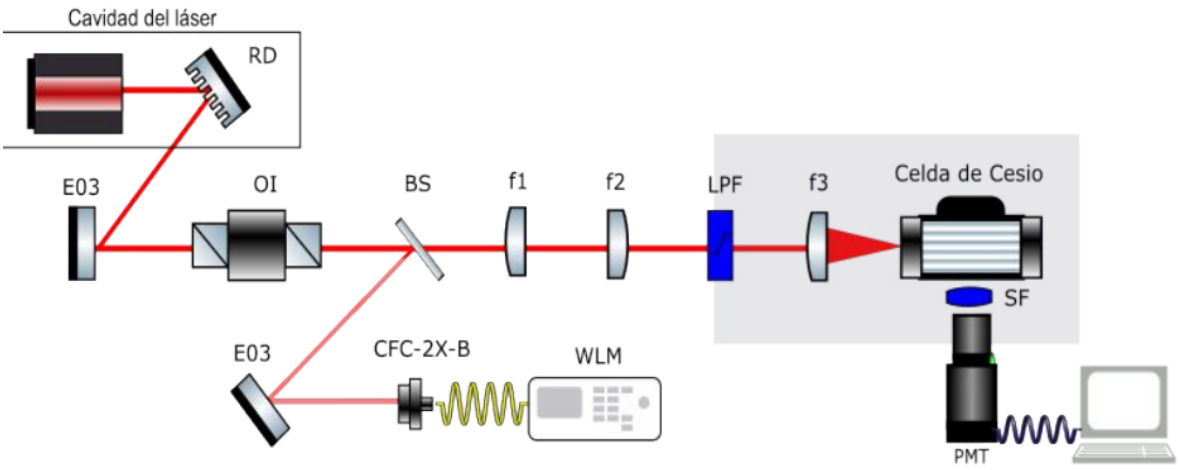

FIG. 3. Schematic of the experimental setup for Doppler-broadened TPA with linear polarization. RD: Littrow diffraction grating; E03: dielectric mirrors; OI: optical isolator; BS: beam sampler; CFC-2X-B: fiber coupler; WLM: wavelength meter; f_1, f_2: divergent telescope lenses; LPF: long-pass filter; f_3: focusing lens; SF: spectral filter; PMT: photomultiplier tube.

C. Doppler-free TPA – linear and circular polarization

The DF configurations share the same input arm as the DB scheme. A high-reflectivity mirror placed behind the cesium cell retroreflects the beam back through the cell, producing the counter-propagating geometry required for Doppler cancellation, Eqs. (4)– (5). An additional lens equal to f_3 is placed between the cell and the mirror to re-focus the retroreflected beam onto the same waist as the forward beam, maximizing the overlap of the two counter-propagating modes inside the excitation volume. The overall arrangement is shown in Fig. 4.

For the *linear-polarization* DF scheme the two quarter-wave plates indicated in Fig. 4 are removed; both beams remain π-polarized ($m = 0$), so the selection rule $m_1 + m_2 = 0$ is automatically satisfied for any combination of photons. The fluorescence spectrum then contains a narrow Doppler-free peak at the resonance frequency sitting on top of the residual Doppler-broadened background produced by atoms that absorb two photons from the same beam.

For the *circular-polarization* DF scheme, a quarter-wave plate ($\lambda/4$) is placed between the LPF and the cell to convert the input π-polarized beam into σ^+, and a second $\lambda/4$ plate is placed between the cell and the retroreflecting mirror. The double pass through this second plate ensures that the beam returning into the cell is σ^-. The combination $\sigma^+ \otimes \sigma^-$ satisfies $m_1 + m_2 = 0$

and drives the transition, while the co-propagating combinations $\sigma^+ \otimes \sigma^+$ or $\sigma^- \otimes \sigma^-$ would give $m_1 + m_2 = \pm 2$ and are suppressed by the selection rules. As a result, the broad Doppler pedestal is strongly attenuated and the spectrum is dominated by the narrow Doppler-free peak.

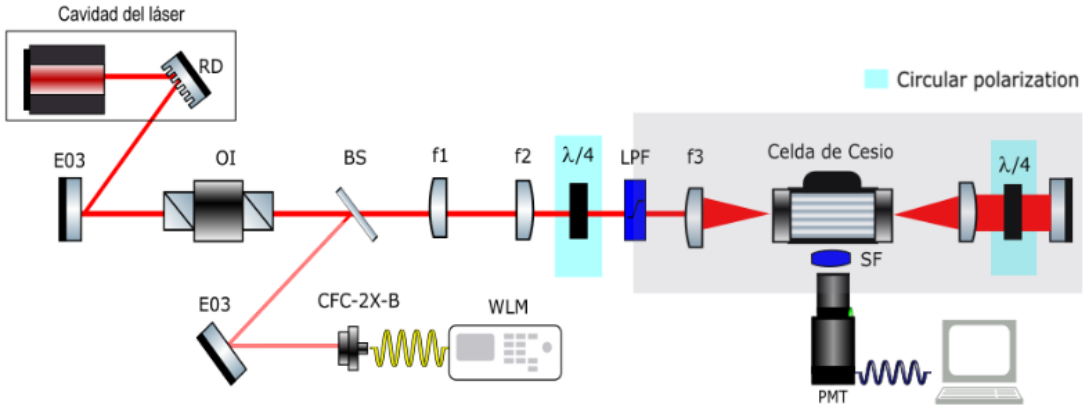

FIG. 4. Schematic of the experimental setup for Doppler-free TPA. The optical chain up to the cesium cell is identical to that of Fig. 3. A retroreflecting mirror behind the cell and a refocusing lens generate the counter-propagating geometry required for Doppler-free excitation. For the linear-polarization scheme the two $\lambda/4$ plates are removed; for the circular-polarization scheme they are inserted before and after the cell to produce the $\sigma^+ \otimes \sigma^-$ combination that satisfies the selection rule $m_1 + m_2 = 0$ while suppressing the co-propagating absorption.

D. Data acquisition and fitting procedure

In every configuration the laser frequency is scanned across the $6S_{1/2} \rightarrow 8S_{1/2}$ resonance while the PMT counts are recorded and tagged with the instantaneous wavelength reported by the WLM. Each spectrum is the average of several scans to reduce statistical noise.

The fluorescence spectra are fitted to the following functional forms:

- **DB, linear polarization:** a single Gaussian profile,

$$F_{\mathrm{DB}}(\nu) \;=\; A_G \exp\!\left[-4\ln 2\,\frac{(\nu-\nu_0)^2}{\Gamma_G^2}\right] + B, \tag{6}$$

  where Γ_G is the Gaussian FWHM, A_G the peak amplitude, ν_0 the resonance frequency and B a background offset.

- **DF, linear polarization:** the sum of a broad Gaussian (Doppler pedestal from co-propagating absorption) and a narrow Lorentzian (Doppler-free peak),

$$F_{\mathrm{DF}}^{\mathrm{lin}}(\nu) \;=\; A_G\, e^{-4\ln 2\,(\nu-\nu_0)^2/\Gamma_G^2} \;+\; \frac{A_L\,(\Gamma_L/2)^2}{(\nu-\nu_0)^2+(\Gamma_L/2)^2} \;+\; B. \tag{7}$$

- **DF, circular polarization:** a single Lorentzian on a flat background,

$$F_{\mathrm{DF}}^{\mathrm{circ}}(\nu) \;=\; \frac{A_L\,(\Gamma_L/2)^2}{(\nu-\nu_0)^2+(\Gamma_L/2)^2} + B. \tag{8}$$

From the Gaussian FWHM obtained in the DB scheme, the cell temperature is inferred by inverting Eq. (3),

$$T \;=\; \frac{Mc^2}{8k_B\ln 2}\left(\frac{\delta\omega_D}{\omega_{fi}}\right)^2. \tag{9}$$

The natural linewidth of the $8S_{1/2}$ state used as a reference is $\gamma_f = 9.62\times10^6$ s^{-1}, obtained from the lifetime $\tau = 104$ ns of the $8S_{1/2}$ state [12], corresponding to $\mathrm{FWHM_{nat}} = \gamma_f/(2\pi) = 1.53$ MHz.

For the temperature-dependent study, the DF (linear polarization) fluorescence spectrum is recorded at six cell temperatures between 22°C and 50°C. For each temperature, the maximum of the fluorescence signal is extracted and plotted against temperature to characterize how the DF peak intensity scales with the cesium vapor density.

III. RESULTS AND ANALYSIS

A. Doppler-broadened TPA with linear polarization

Figure 5 shows the fluorescence spectrum recorded in the DB configuration with linear polarization at a nominal cell temperature $T_{\mathrm{set}} = 45°\mathrm{C} = 318.15$ K. The data is well described by a single Gaussian profile, Eq. (6), yielding a coefficient of determination $R^2 = 0.986$ and a FWHM of

$$\Gamma_G^{\mathrm{DB}} \;=\; (808 \pm 3)\ \mathrm{MHz}.$$

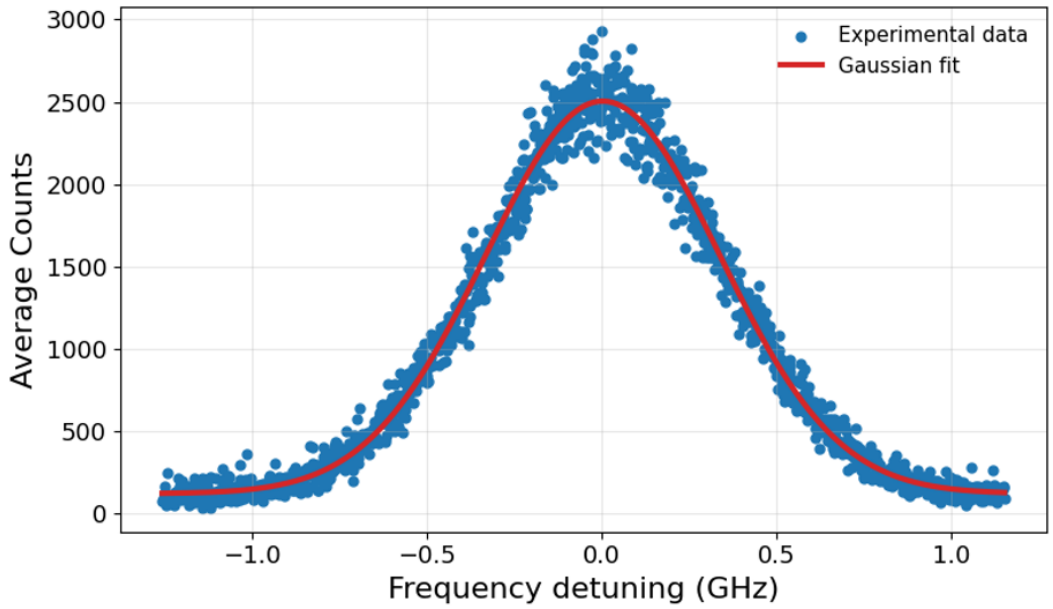

FIG. 5. Doppler-broadened two-photon induced fluorescence spectrum for the $6S_{1/2} \rightarrow 8S_{1/2}$ ($F = 4 \rightarrow F = 4$) transition with linear polarization at $T_{\rm set} = 45°$C. Blue points: experimental data. Solid line: Gaussian fit, Eq. (6). A frequency detuning of 0 represents the fitted resonance wavelength $\lambda_0 \approx 822.4689$ nm.

The measured width contains a small contribution from the natural Lorentzian linewidth (1.53 MHz). Subtracting this contribution in quadrature, the pure Doppler component is $\Delta\nu_D \simeq 806.62$ MHz. Substituting in Eq. (9) gives an experimentally inferred cell temperature

$$T_{\rm exp} \;=\; (318.3 \pm 2.4)\ {\rm K} \;=\; (45.2 \pm 0.8)°{\rm C},$$

in excellent agreement with the set-point $T_{\rm set} = 45°$C and consistent with the Doppler width previously reported for this transition in Cs near room temperature [5].

B. Doppler-free TPA with linear polarization

When the retroreflecting mirror and the refocusing lens are inserted, a narrow Doppler-free feature appears at the center of the Doppler-broadened pedestal, as predicted by Eqs. (4)–(5). The spectrum is shown in Fig. 6 together with the combined Gaussian + Lorentzian fit of Eq. (7).

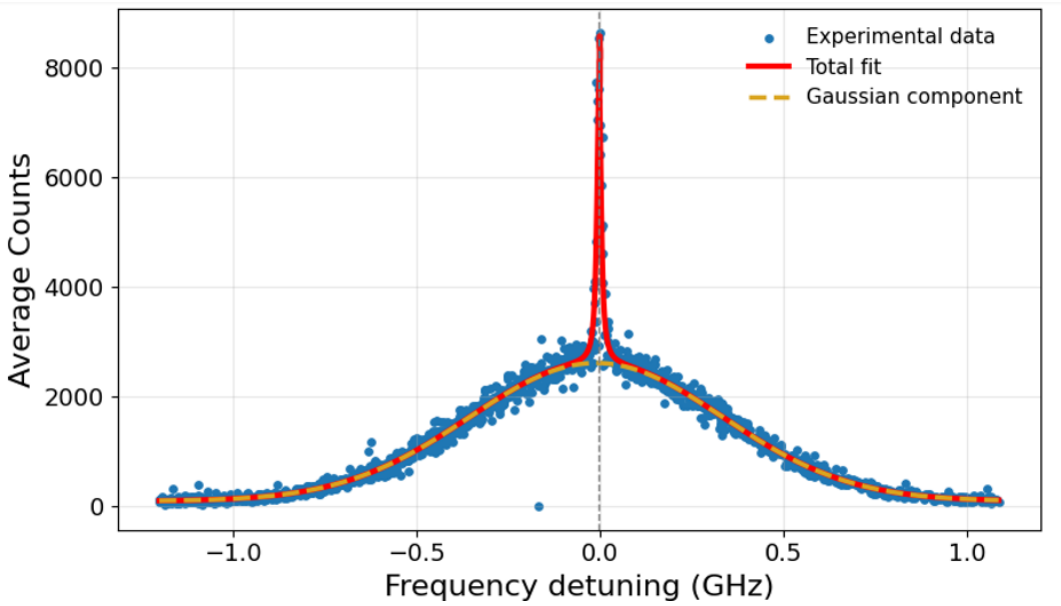

FIG. 6. Doppler-free fluorescence spectrum with linear polarization at $T_{\text{set}} = 45°\text{C}$. Blue points: experimental data. Dashed orange line: Gaussian component (residual Doppler pedestal). Solid red line: combined Gaussian + Lorentzian fit, Eq. (7). The narrow central peak corresponds to the Doppler-free contribution from counter-propagating photons.

The total fit gives $R^2_{\text{tot}} = 0.961$, with a Lorentzian FWHM of

$$\Gamma_L^{\text{DF,lin}} \;=\; (5.96 \pm 0.01)\ \text{MHz},$$

which is about 4.43 MHz above the natural linewidth of 1.53 MHz. The residual broadening has several contributions. The dominant one is the optical feedback from the retroreflecting arm into the laser cavity: with the counter-propagating geometry well aligned, a non-negligible fraction of the back-reflected light couples back into the laser through the single optical isolator available in the setup, perturbing its emission frequency and reducing its stability between successive scans. This effectively broadens the laser linewidth seen by the atoms and introduces a shot-to-shot drift of the central frequency, both of which inflate the apparent FWHM of the fitted Lorentzian. On top of this, smaller contributions are expected from power broadening at the laser intensities used here, transit-time broadening of the atoms through the focal volume, and residual broadening from magnetic fields and collisions in the thermal cell [6].

Reading the maxima of Figs. 5 and 6 at the same laser power and cell temperature we find

$$\frac{F^{\text{peak}}_{\text{DF,lin}}}{F^{\text{peak}}_{\text{DB,lin}}} \;\approx\; 3{:}1, \tag{10}$$

quantifying the gain produced by Doppler cancellation. Although the theoretical TPA cross-section at resonance is predicted to increase by more than two orders of magnitude when going from the Doppler-broadened to the Doppler-free regime (cf. the values $\widetilde{\sigma}_0^{\mathrm{DF}} = 1.23 \times 10^{-21}$ cm^4/W and $\widetilde{\sigma}_0^{\mathrm{DB}} = 3.65 \times 10^{-24}$ cm^4/W reported for this transition in Ref. [5]), the observed factor of ~ 3 already confirms that the implementation moves in the expected direction. The fluorescence peak is enhanced relative to the purely Doppler-limited case, demonstrating that the counter-propagating geometry is an effective route to increase the count rate in the two-photon induced fluorescence signal. Closing the gap between the observed ratio and the maximum predicted enhancement will require, among other refinements, a better beam-waist overlap of the two counter-propagating modes inside the cell, reduction of optical feedback, and a narrower laser linewidth.

C. Doppler-free TPA with circular polarization

Inserting the two $\lambda/4$ plates before and after the cell selects the $\sigma^+ \otimes \sigma^-$ counter-propagating combination and suppresses the absorption of two co-propagating photons of the same helicity, which would violate the selection rule $m_1 + m_2 = 0$. The broad Doppler pedestal is strongly attenuated, and the fluorescence spectrum becomes essentially a pure Lorentzian sitting on a flat background, as shown in Fig. 7.

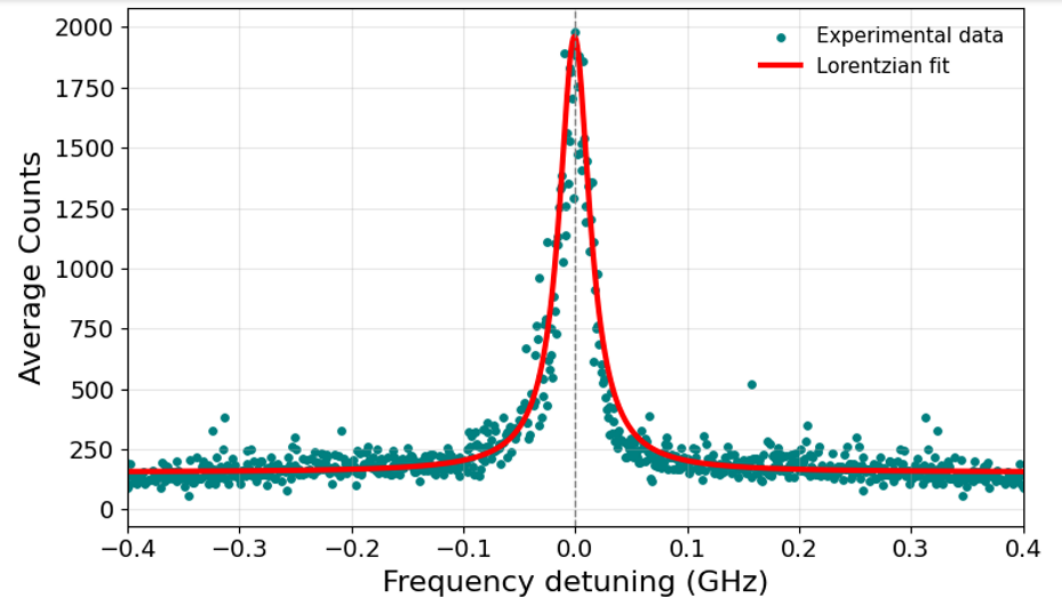

FIG. 7. Doppler-free fluorescence spectrum with circular polarization ($\sigma^+ \otimes \sigma^-$) at $T_{\rm set} = 45°$C. Blue points: experimental data. Solid red line: Lorentzian + background fit, Eq. (8). The Doppler-broadened pedestal observed in Fig. 6 is suppressed by the selection rules.

The Lorentzian fit gives $R^2 = 0.880$ and

$$\Gamma_L^{\rm DF,circ} \;=\; (10.14 \pm 0.01)\ \text{MHz},$$

i.e. 8.61 MHz above the natural linewidth. As in the linear-polarization case, the residual broadening is dominated by optical feedback from the retroreflecting arm into the laser cavity through the single optical isolator available in the setup, which perturbs the laser frequency and reduces its stability between successive scans. The effect is more severe in the circular-polarization configuration: the additional quarter-wave plates after the cell produce extra surfaces from which light can be back-reflected into the laser, increasing the overall amount of feedback and degrading both the apparent linewidth and the fit quality. Reducing this optical feedback, for example by adding a second optical isolator or by slightly misaligning the retroreflected beam from perfect back-coupling, is expected to bring the measured linewidth closer to the natural-linewidth limit in both configurations.

D. Temperature dependence of the Doppler-free peak

To characterize how the DF fluorescence amplitude scales with the cesium vapor density, the DF (linear-polarization) spectrum was recorded at six cell temperatures between 22°C and 50°C. The full spectra are overlaid in Fig. 8; the maximum fluorescence as a function of temperature is shown in Fig. 9.

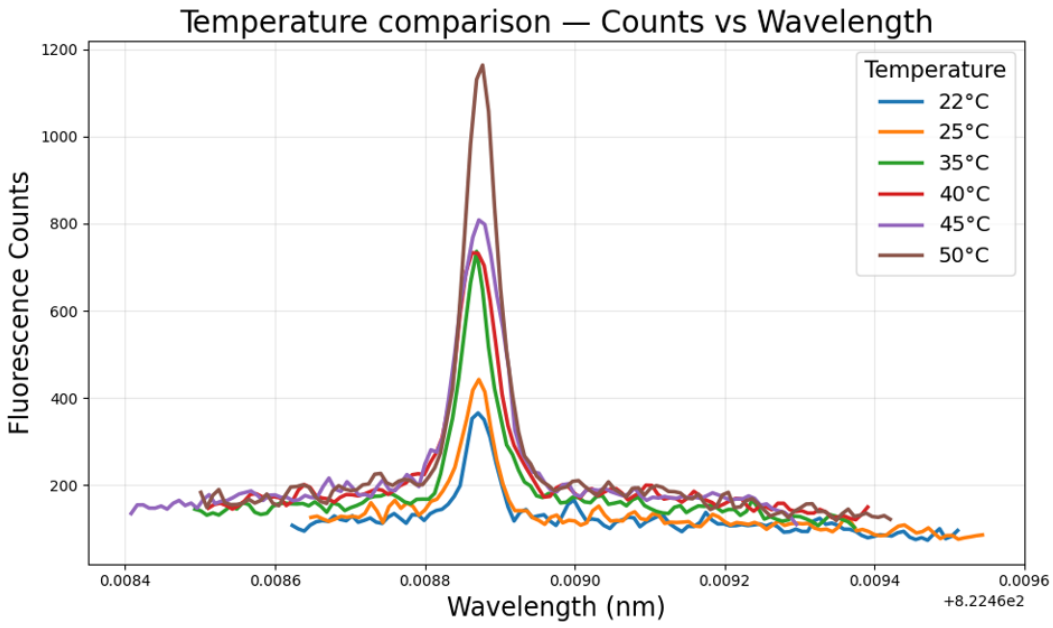

FIG. 8. Doppler-free fluorescence spectra (linear polarization, counter-propagating beams) measured at cell temperatures between 22°C and 50°C.

The peak fluorescence increases monotonically with temperature in the explored range. This trend is consistent with the rapid growth of the saturated cesium vapor pressure with temperature [11]: in this temperature window the atomic number density inside the cell increases by roughly an order of magnitude, which translates into a larger TPA rate in the excitation volume because the total number of ground-state atoms available for the transition scales linearly with N (cf. Eq. (18) of Ref. [5]). A quantitative comparison with the saturated-vapor-pressure prediction requires a more accurate measurement of the cell temperature than that provided by the heater read-back used here, and is left for future work.

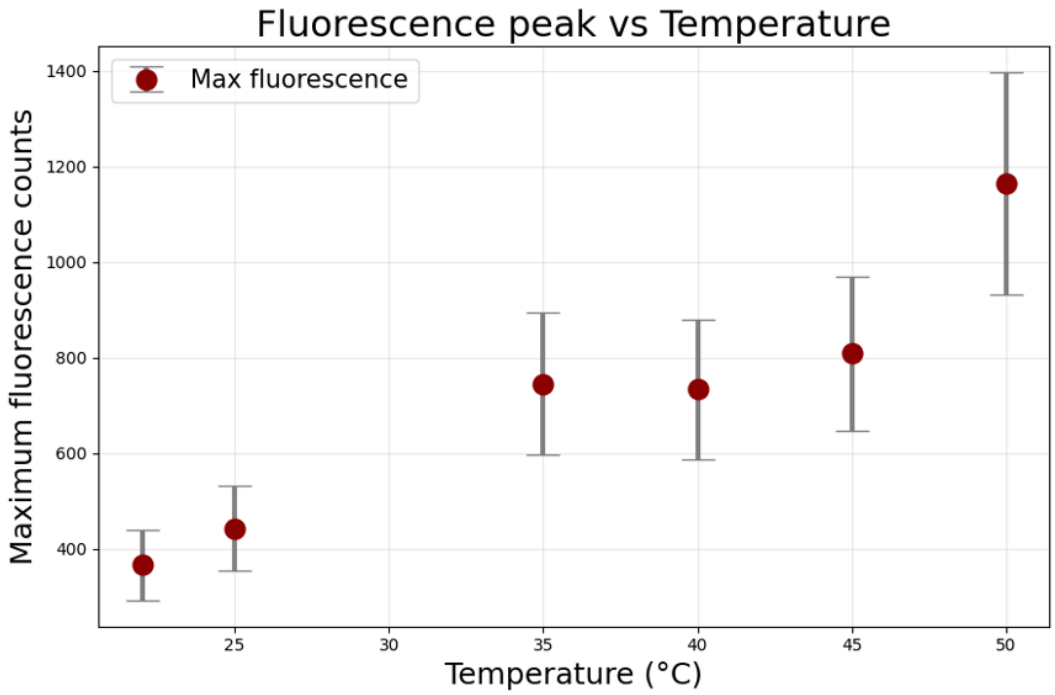

FIG. 9. Maximum of the Doppler-free fluorescence peak as a function of cell temperature, extracted from the spectra of Fig. 8. The error bars represent the statistical uncertainty obtained from repeated scans at each temperature.

E. Summary of the comparison

Table I summarizes the main quantitative results obtained in this work, comparing the three configurations in terms of peak amplitude and FWHM. The DF schemes deliver a narrower line and a larger peak fluorescence than the DB scheme, in agreement with the expected behavior [8].

TABLE I. Summary of the spectral parameters extracted in this work for the cesium $6S_{1/2} \rightarrow 8S_{1/2}$ two-photon transition at $T_{\mathrm{set}} = 45°\mathrm{C}$. The natural linewidth of the upper state is 1.53 MHz [12].

Configuration	Fit	FWHM	R^2
DB, linear polarization	Eq. (6)	(808 ± 3) MHz	0.986
DF, linear polarization	Eq. (7)	(5.96 ± 0.01) MHz	0.961
DF, circular polarization	Eq. (8)	(10.14 ± 0.01) MHz	0.880

The transition from the DB to the DF regime reduces the measured FWHM by more than two orders of magnitude, from ~ 800 MHz down to a few MHz, demonstrating that the Doppler cancellation provided by the counter-propagating geometry works as expected. The two DF measurements

remain above the natural-linewidth limit of 1.53 MHz: by a factor of ~ 4 in the linear-polarization case and by a factor of ~ 7 in the circular-polarization case. The progressive degradation of the fit quality from $R^2 = 0.986$ (DB) to $R^2 = 0.961$ (DF, linear) and $R^2 = 0.880$ (DF, circular) is consistent with the increasing impact of optical feedback into the laser cavity, which is more severe in the configurations involving retroreflection of the beam and additional optical surfaces in the return path. Taken together, the three measurements show that the DF schemes are effective at narrowing the line and enhancing the fluorescence peak relative to the DB case, while also identifying the dominant residual error source that limits the present implementation and that future improvements should address.

IV. CONCLUSIONS

We have implemented and compared Doppler-broadened and Doppler-free two-photon excitation of the $6S_{1/2} \rightarrow 8S_{1/2}$ transition in a cesium vapor cell at 822 nm. In the Doppler-broadened configuration with linear polarization, the fluorescence spectrum is well described by a Gaussian of FWHM (808±3) MHz, from which the cell temperature is inferred to be (318.3±0.8) K, in excellent agreement with the set point $T_{\mathrm{set}} = 45°\mathrm{C}$. This validates both the calibration of the experimental setup and the description of the line shape by Eq. (3).

When the cell is illuminated by two counter-propagating beams, a narrow Doppler-free feature appears at the resonance frequency. With linear polarization the spectrum is described by a Gaussian pedestal plus a Lorentzian of FWHM (5.96 ± 0.01) MHz, and the ratio of peak fluorescence between the DF and DB schemes is $\sim 3:1$. Although this gain is below the more than two orders of magnitude predicted from the theoretical Doppler-free and Doppler-broadened cross-sections reported in Ref. [5], the observed enhancement confirms that the counter-propagating geometry is moving the experiment in the expected direction and provides a concrete handle to increase the fluorescence count rate. With circular polarization ($\sigma^+ \otimes \sigma^-$), the broad Doppler pedestal is suppressed by the selection rule $m_1 + m_2 = 0$, the spectrum becomes essentially Lorentzian, and the FWHM is (10.14 ± 0.01) MHz. The temperature-dependent study of the DF signal between 22°C and 50°C shows that the peak fluorescence grows monotonically with the cesium vapor density, consistent with the temperature dependence of the saturated vapor pressure [11].

The residual widths of the Doppler-free features (~ 4 MHz and ~ 9 MHz above the natural linewidth of 1.53 MHz in the linear and circular cases, respectively) and the progressive degradation

of the fit quality from $R^2 = 0.986$ in the DB scheme down to $R^2 = 0.880$ in the DF circular scheme indicate that the experiment is currently limited by optical feedback from the retroreflecting arm into the laser cavity through the single optical isolator available in the setup. This feedback effectively broadens the laser linewidth seen by the atoms and introduces a shot-to-shot drift of the central frequency, and its impact is more severe in the circular-polarization configuration because of the additional optical surfaces of the quarter-wave plates in the return path. Smaller contributions from power broadening, transit-time broadening and residual broadening from magnetic fields and collisions are also expected, but are subdominant compared to the laser-feedback effect under the present conditions.

Future improvements will focus on reducing the optical feedback into the laser, for example by adding a second optical isolator or by slightly misaligning the retroreflected beam from perfect back-coupling, and on optimizing the overlap of the two beam waists inside the cell to maximize the DF/DB amplitude ratio. A more accurate, independent measurement of the cell temperature will also be required to quantitatively model the dependence of the fluorescence signal on the cesium vapor density. With these refinements, the gain in peak fluorescence demonstrated here can be pushed toward its theoretical upper bound, paving the way for two-photon spectroscopy in cesium at the low-photon-flux regime relevant to entangled two-photon absorption (ETPA), where reliable fluorescence detection is the limiting factor [9].

---

[1] M. Göppert-Mayer, "Über Elementarakte mit zwei Quantensprüngen," *Ann. Phys.* **401**, 273–294 (1931).

[2] R. W. Boyd, *Nonlinear Optics*, 4th ed. (Academic Press, 2020).

[3] C. Xu and W. W. Webb, "Measurement of two-photon excitation cross sections of molecular fluorophores with data from 690 to 1050 nm," *J. Opt. Soc. Am. B* **13**, 481–491 (1996).

[4] F. Biraben, "The first decades of Doppler-free two-photon spectroscopy," *C. R. Phys.* **20**, 671–681 (2019).

[5] M. Caracas Núñez, M. A. Gonzalez, and M. Núñez Portela, "Theoretical and experimental study of the 6S–8S two-photon absorption cross-section in cesium atoms," *Opt. Express* **31**, 31749–31759 (2023).

[6] W. Demtröder, *Laser Spectroscopy 1: Basic Principles*, 5th ed. (Springer, 2014).

[7] G. Grynberg and B. Cagnac, "Doppler-free multiphotonic spectroscopy," *Rep. Prog. Phys.* **40**, 791–841 (1977).

[8] V. Jacques, B. Hingant, A. Allafort, M. Pigeard, and J. F. Roch, "Nonlinear spectroscopy of rubidium: an undergraduate experiment," *Eur. J. Phys.* **30**, 921–932 (2009).

[9] M. S. Caracas Núñez, *Theoretical & Experimental Entangled Two-Photon Absorption in Cesium Atoms*, M.Sc. thesis, Universidad de los Andes, Bogotá, 2025.

[10] A. J. Olson, E. J. Carlson, and S. K. Mayer, "Two-photon spectroscopy of rubidium using a grating-feedback diode laser," *Am. J. Phys.* **74**, 218–223 (2006).

[11] C. B. Alcock, V. P. Itkin, and M. K. Horrigan, "Vapour pressure equations for the metallic elements: 298–2500 K," *Can. Metall. Q.* **23**, 309–313 (1984).

[12] G. Alessandretti, F. Chiarini, G. Gorini, and F. Petrucci, "Measurement of the Cs 8S-level lifetime," *Opt. Commun.* **20**, 289–291 (1977).